Available online at www.sciencedirect.com

SciVerse ScienceDirect

Journal of the European Ceramic Society 32 (2012) 689–696

www.elsevier.com/locate/jeurceramsoc

# The role of Ce reduction in the segregation of metastable phases in the $ZrO_2$–$CeO_2$ system

M.L. Sanjuán [a,*], P.B. Oliete [a], A. Várez [b], J. Sanz [c]

[a] *Instituto de Ciencia de Materiales de Aragón, Universidad de Zaragoza-CSIC, Facultad de Ciencias, Universidad de Zaragoza, 50009 Zaragoza, Spain*
[b] *Dpto. de Materiales, IAAB, Universidad Carlos III de Madrid, 28911 Leganés, Spain*
[c] *Instituto de Ciencia de Materiales de Madrid, CSIC, Cantoblanco, 28049 Madrid, Spain*

Received 11 July 2011; received in revised form 27 September 2011; accepted 1 October 2011
Available online 27 October 2011

**Abstract**

The complexity of the $ZrO_2$–$CeO_2$ phase diagram arises from several factors: the low solubility of each compound into the other one, the slow kinetics of cation diffusion, the occurrence of Ce reduction at high temperatures, and the existence of several metastable phases whose appearance and evolution depend on synthesis method and thermal history of the sample. Identification of phase content is moreover complicated because the X-ray diffractograms of some $ZrO_2$–$CeO_2$ phases are very close or even indistinguishable, which imposes the use of other techniques more sensitive to small oxygen displacements. In this work we present a Raman spectroscopic study of phase segregation in the $ZrO_2$–$CeO_2$ system between 1300 and 1650 °C, focusing on the effect of Ce reduction at high temperatures and its relation with the appearance of metastable phases upon cooling. The nature of the high-temperature defective cubic phase is discussed.


*Keywords:* Phase diagrams; $CeO_2$; $ZrO_2$; Diffusion; Defects; Spectroscopy

## 1. Introduction

Ce-based materials have a wide spectrum of technological applications, most of which are based on the well-known redox properties of the $Ce^{4+}/Ce^{3+}$ pair (see Ref. 1 for a recent review). Among Ce-related capabilities, oxygen storage, which is the basis of operation of automotive catalysts,[2,3] takes advantage of the simultaneous and reversible occurrence of oxygen loss (or retrapping) and cerium reduction (or oxidation) in Ce-based oxides. It is known that the addition of $ZrO_2$ to ceria improves the oxygen storage capacity (OSC) of $CeO_2$ as well as its stability against sintering.[4,5] For catalysis, homogeneous $Zr_{1-x}Ce_xO_2$ solid–solutions with high surface area are desirable. These, however, are not equilibrium phases of the $ZrO_2$–$CeO_2$ (ZCO) system, except for close-to-the-end compositions. The limited solubility of $ZrO_2$ in $CeO_2$ and vice versa, together with the need of high surface materials, imposes the use of low temperature synthesis methods, which yield metastable $Zr_{1-x}Ce_xO_2$ solid–solutions with the desired composition.[6] An important issue in these cases is chemical inhomogeneity, since it affects the OSC and thermal stability.[7] Even in samples that appear to be single-phase at the X-ray diffraction (XRD) level, there exists nanometer-scale inhomogeneity that favors unwanted crystallite growth and phase segregation upon heating at moderate temperatures (∼900 °C).[8–10]

The strict conditions required for technical applications of the ZCO systems have led to intense research on the production, processing and characterization of these oxides. Some aspects of the $ZrO_2$–$CeO_2$ phase diagram (PD), however, are still under debate, despite an enormous number of studies. Several factors contribute to unexpected complexity:

First, the end compounds are not isomorphous: $CeO_2$ adopts the well-known cubic fluorite phase (space group $Fm\text{-}3m$) at all temperatures, whereas the equilibrium phase of pure $ZrO_2$ at RT is monoclinic with space group $P2_1/c$. There is no mutual solubility of $CeO_2$ in $ZrO_2$ at RT and vice versa, except for very low percentages. According to the widely accepted equilibrium PD established by Yashima et al. in a series of papers,[11–16] (see Fig. 1), phase separation occurs at intermediate compositions

* Corresponding author. Tel.: +34 976761000x3354; fax: +34 976761229.
*E-mail addresses:* sanjuan@unizar.es (M.L. Sanjuán), poliete@unizar.es (P.B. Oliete), alvar@ing.uc3m.es (A. Várez), jsanz@icmm.csic.es (J. Sanz).

0955-2219/$ – see front matter © 2011 Elsevier Ltd. All rights reserved.
doi:10.1016/j.jeurceramsoc.2011.10.015

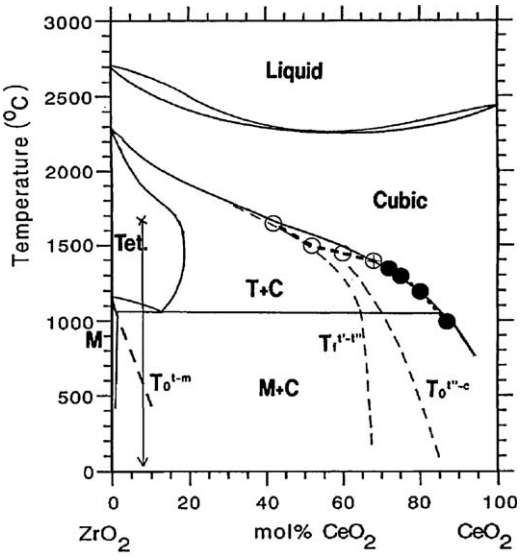


Fig. 1. $ZrO_2$–$CeO_2$ phase diagram, according to Yashima et al.,[11–16] (figure adapted from Ref. 16) and Ce content in the Ce-rich segregated phase derived from Raman results presented in this work. ◯: $t'$ phase; ⊕: $t''$ phase; ●: cubic phase. Continuous and dashed lines represent the equilibrium and metastable phase diagrams, respectively. Dotted line is only a guide for the eye. The error in the determination of Ce concentration is approx. ±0.02.

between a Ce-poor, monoclinic phase ($x<5\%$), and a Ce-rich, cubic fluorite phase, $c$, whose Ce concentration varies from a content above 95% at RT to 85% at 1050 °C. At that temperature there exists an eutectoid reaction; for $T>1050$ °C phase segregation occurs for nominal cerium contents above 15% in the form of a tetragonal phase, $t$, with ∼15–20% Ce content and a Ce-rich, cubic phase whose Ce composition decreases very fast with increasing temperature.

Intermediate $Zr_{1-x}Ce_xO_2$ compositions may form as metastable phases, and these in turn may be cation ordered or disordered. Fluorite-like, cation disordered phases are obtained after long-period annealing at high temperature (above the $t+c$ segregation field) in an oxidizing or slightly reducing atmosphere. As reported by Yashima et al., in these conditions defective cubic phases are formed, that may be quenched by fast cooling. Upon mild reoxidation treatments, oxygen stoichiometry is recovered but then the samples transform to metastable tetragonal structures $t'$ or $t''$, or monoclinic $m'$ phase, depending on the Ce content. The range of $t'$ phase extends from 15% to ∼68% at RT, whereas the pseudocubic $t''$ phase forms from ∼68% to 90%. Upon fast heating (to prevent segregation), $t''$ phase transforms to cubic phase, whereas $t'$ phase transforms first into $t''$ and then into cubic phase. These transitions are represented by dashed lines in Yashima's PD (Fig. 1).

Metastable $t'$ and $t''$ phases may also form after low temperature synthesis, due to surface/size effects. In that case the range of appearance of $t'$ and $t''$ phases differs from that obtained through high temperature annealing, and pseudocubic phases may be found even for $x=0.5$ compositions.[10,17]

Severe reduction at high temperatures (typically higher than 1100 °C) yields almost full $Ce^{4+}$ to $Ce^{3+}$ conversion and, for compositions close to $x=0.5$, cation order occurs to form pyrochlore-like $Ce_2Zr_2O_{7+\delta}$. Upon mild reoxidation at $T\sim600$ °C, a fully stoichiometric $Ce_2Zr_2O_8$ cubic phase is recovered, usually denoted as $\kappa$-$Ce_2Zr_2O_8$.[18] Cation-ordered phases with intermediate compositions present improved OSC properties with respect to $CeO_2$, notably at low temperature.[19] A variety of other tetragonal metastable phases, such as those labeled $t^*$ and $t'$-meta, can be found upon varying reduction and reoxidation temperatures.[18] These cation disordered phases are hard to distinguish from the usual $t'$ phase by XRD, since they differ only in slight differences of the oxygen $z$ coordinate, but can be identified by Raman spectroscopy.[18]

Since most applications of ZCO compounds involve Ce redox processes, it is mandatory to know how these materials behave in different environments; in particular which is the influence of Ce reduction in phase segregation at moderate or high temperatures. In this work we use Raman scattering to investigate phase separation for intermediate compositions of the $ZrO_2$–$CeO_2$ system sintered in the 1300–1650 °C temperature range, focusing in reduction effects and their influence in the appearance of metastable phases. Though at these temperatures low surface area (LSA) materials are formed, less interesting for catalytic purposes than high surface area (HSA) systems, there are several aspects that justify this study. First, it has been shown that in mixed $ZrO_2$–$CeO_2$ oxides redox processes responsible for OSC are mediated by oxygen conduction and occur mostly in the bulk,[20] so that studying reduction related features in LSA samples, free from surface effects, is also useful, even if their catalytic activity is worse. Moreover, phase identification upon oxygen uptake or release may be complicated in HSA systems due to the broad diffractograms obtained in these samples. Size effects are also responsible for the appearance of metastable phases in HSA systems, which may obscure similar effects arising from Ce reduction.

The usefulness of Raman scattering in ceria–zirconia systems is based on its sensitivity to small oxygen displacements, which allows distinguishing between phases that present almost identical XRD patterns, such as the already mentioned metastable $t'$, $t'$-meta or $t^*$ phases, or between the cubic and pseudocubic ($t''$) phases. Before the latter was identified by Yashima et al. by means of Raman spectroscopy, first in $Zr_{1-x}Y_xO_{2-x/2}$ (Ref. 21) and then in the ZCO system,[12] both phases were assumed to share similar, fluorite-like structure. Thus, in a previous XRD characterization of compositions with $x\geq0.6$ annealed at 1650 °C,[22] a single cubic phase was found, though it was evident that some of those "cubic" phases where probably pseudocubic ones. Raman spectroscopy is also valuable in detecting nanoscale structural or chemical inhomogeneity. This is especially important in HSA systems, where diffractogram broadening may mask small tetragonal splittings, or even the coexistence of several phases with close lattice parameters. Moreover, the strong variation of Raman shifts and intensities along the $Zr_{1-x}Ce_xO_2$ series allows using it to identify the composition and phase content of the sample. An alternative approach for phase identification is attempted in Ref. 23 by using Eu(III) luminescence as a probe of local symmetry.

In this work, phase attribution is made on the basis of peak frequencies and relative intensities. Several bands are especially critical for phase identification, due to their strong $\nu(x)$ dependence. Thus, monoclinic $ZrO_2$ is easily identified by a doublet at 183–193 $cm^{-1}$ (Ref. 24); tetragonal phase stable at high temperature presents always an intense band around 250 $cm^{-1}$, as well as a triplet of high frequency bands in the region of 630 $cm^{-1}$.[24] At the Ce-rich end, cubic fluorite gives a huge peak at 465–472 $cm^{-1}$, with a weak shoulder at higher frequency due to defects, and almost no intensity in the low frequency side.[12] The metastable $t'$ phase can be identified by the downward shift of the originally $t$-like band from 250 to 160 $cm^{-1}$ as $x$ is increased, and also by the aspect of the band at 455–470 $cm^{-1}$ and its high frequency wing.[12] The identification of the metastable $t''$-phase is more subtle, since it also results in an intense pseudocubic band close to that of cubic fluorite. However, the spectrum can be differentiated by the higher frequency of the pseudocubic band (473–480 $cm^{-1}$) and also by the weak band that appears around 300 $cm^{-1}$, due to oxygen off-center location.[12] No cation-ordered phases were found in this study, neither other $t'$-related phases such as $t'$-meta or $t^*$, so that the Raman spectra of these phases is not described here.

For the conditions used in this work the error in the determination of phase composition through Raman spectra is estimated to be approx. 2%, i.e., the error bar for Ce content $x$ is $x \pm 0.02$. Though Raman scattering provides accurate phase identification, quantitative determination of relative phase content is difficult, unless precise measurements with reference samples are available. This task has not been attempted in this work.

## 2. Experimental details

Standard ceramic synthesis was used, starting from the mixture of reagent oxides $CeO_2$ and $ZrO_2$. Pellets of nominal composition $Zr_{1-x}Ce_xO_2$, with $x = 0.2$, 0.4, 0.5, 0.6, and 0.8, were annealed at 1500 and 1650 °C during 12 or 24 h. Two other compositions ($x = 0.7$, 0.9) were also annealed at 1650 °C. [We shall use the notation Ce$x$ for material with the nominal composition $(ZrO_2)_{1-x}(CeO_2)_x$.] A set of $Ce_{0.4}$ samples were further submitted to a sequence of annealing temperatures ($T_a$) during 12 h: $T_a$ = 1300 °C, 1350 °C, 1400 °C, 1450 °C, 1500 °C and 1650 °C. Annealing at 1300 °C during 24 h was also performed. The heating and cooling rates used in the thermal treatments were 1 °C $min^{-1}$. XRD patterns of most samples were recorded with the CuKα radiation, by using the ($\theta/2\theta$) Bragg–Brentano geometry, in an X'Pert Philips instrument equipped with a curved graphite monochromator. The diffractogram of the sample annealed at 1500 °C was recorded in a D-Max Rigaku equipment using also CuKα lines.

Room temperature Raman spectra were recorded in a DILOR XY spectrometer equipped with a liquid nitrogen-cooled Charge-Coupled Device (CCD) detector. Excitation was performed through the 50× objective lens of a microscope, using the 514.5 nm line of an $Ar^+$ laser. The Si mode at 520 $cm^{-1}$ was used for frequency calibration.

## 3. Experimental results

Fig. 2 shows the X-ray diffractogram of $Ce_{0.4}$ samples annealed at increasing temperatures, from 1350 to 1500 °C. At a first glance it becomes evident that there is coexistence of at least two phases with significantly different lattice parameters, hence with different Ce content. For samples annealed at 1350 °C and 1400 °C we can easily identify diffraction peaks of a cubic (or pseudocubic) $c$ phase and those of a tetragonal $t$ phase that we ascribe, according to the $ZrO_2$–$CeO_2$ phase diagram, to Ce-rich and Ce-poor segregated phases, respectively. Inspection of diffractograms of samples annealed at 1450 and 1500 °C evidences some splitting in the region pertaining to the Ce-rich phase that prevent interpreting them simply as a superposition of $c + t$ phases. Lattice parameters obtained from fitting the diffractograms by means of Fullprof package[25] are given in Table 1. Two phases, $t + c$, were used for $T_a$ = 1350 and 1400 °C, whereas $t + t'$ phases were used for $T_a$ = 1450 and 1500 °C. (Some amount of unreacted $ZrO_2$ and $CeO_2$ oxides was still present in the sample annealed at 1300 °C. On the other hand, the sample annealed at 1650 °C contained a third, Ce-rich cubic phase, besides the $t + t'$ ones.) Fig. 3 shows the pseudocubic lattice parameters, $\bar{a}_c$ and $\bar{a}_t$, of the Ce-rich and Ce-poor segregated phases, respectively, as a function of annealing temperature. The variation of $\bar{a}_t$ follows the Ce-content of the stable tetragonal phase in the 1300–1650 °C temperature interval, whereas the decreasing trend of $\bar{a}_c$ agrees, at least qualitatively, with the decrease in Ce content of the Ce-rich phase in the same temperature interval. Though these data suggest that the sample composition has been preserved upon cooling from high temperature, analysis of phase symmetry and Ce content cannot be made exclusively from XRD data. First, XRD does not distinguish between cubic and $t''$ phases. Second, the presence of tetragonal phases in the Ce-rich side is unexpected. Finally, a unique correspondence between lattice parameter, Ce content and temperature cannot be established. We have included in Fig. 3 lattice parameters of

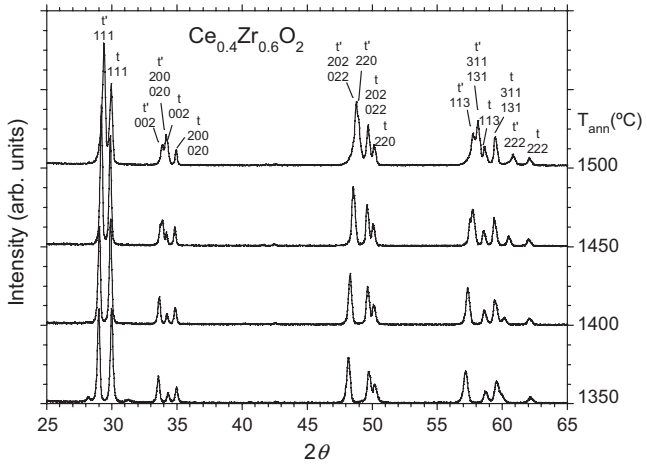


Fig. 2. XRD patterns of nominally $Zr_{0.6}Ce_{0.4}O_2$ samples sintered during 12 h at increasing temperatures, from 1350 to 1500 °C. The patterns can be interpreted as the superposition of two diffractograms, corresponding either to $t + c$ (for $T_a$ = 1350 and 1400 °C) or to two tetragonal phases $t + t'$, for $T_a$ = 1450 and 1500 °C. (See Table 1 for lattice parameters and phase compositions.)

Table 1
Lattice parameters obtained from fitting the X-ray diffractograms by means of Fullprof package. Data for annealing temperatures between 1300 and 1500 °C are obtained from samples of nominal composition $Ce_{0.4}$. Data for $T_a$ = 1650 °C pertain to nominal composition $Ce_{0.3}$; that diffractogram showed a third, cubic phase, with $a$ = 5.3031 Å.

| $T_a$ | Ce-poor phase | | | | Ce-rich phase | | | |
|---|---|---|---|---|---|---|---|---|
| | $a$ | $c$ | $\bar{a}$ | $c/a$ | $a$ | $c$ | $\bar{a}$ | $c/a$ |
| 1300 | 3.6356 | 5.2324 | 3.6571 | 1.0176 | 5.3631 | | 3.7923 | 1 |
| 1350 | 3.6363 | 5.2354 | 3.6582 | 1.0181 | 5.3458 | | 3.7800 | 1 |
| 1400 | 3.6393 | 5.2382 | 3.6608 | 1.0178 | 5.3288 | | 3.7680 | 1 |
| 1450 | 3.6441 | 5.2443 | 3.6655 | 1.0176 | 3.7440 | 5.3223 | 3.7505 | 1.0052 |
| 1500 | 3.6424 | 5.2419 | 3.6638 | 1.0176 | 3.7229 | 5.3097 | 3.7335 | 1.0085 |
| 1650 | 3.6371 | 5.2332 | 3.6582 | 1.0174 | 3.6997 | 5.2922 | 3.7138 | 1.0114 |

samples produced by a modified Pechini method.[10] Differences between both series of samples are attributed to incomplete segregation of Pechini samples, despite only two phases were found in this series. Difficulties inherent to the $ZrO_2$–$CeO_2$ phase diagram mentioned in the introduction (small oxygen-induced distortions, metastable phases, possible reduction at high temperatures) recommend complementing phase identification by other means. As explained, Raman spectroscopy is one of the techniques most sensitive to the peculiarities of this system.

Fig. 4 shows the spectra of $Ce_{0.4}$ samples as a function of increasing annealing temperature, from 1300 to 1650 °C. [The bands between 350 and 420 $cm^{-1}$ are due to luminescence of $Er^{3+}$ impurities.][26] The following stages can be distinguished:

At 1300 and 1350 °C reaction already occurs but it is slow. The phase content of the final product depends on the annealing time, and contains typically weak peaks from the reagent oxides $m$-$ZrO_2$, $c$-$CeO_2$ as well as those of reacted phases $t(x \sim 0.18–0.2)$ and $c(x \sim 0.72–0.75)$.

After 12 h of annealing at 1400 °C the spectra of the starting oxides have disappeared implying that full reaction has occurred. Phase segregation is still observed. However, the strong symmetric peak at 465–470 $cm^{-1}$, typical of Ce-rich phases with cubic fluorite structure, turns into a broader, asymmetric band with maximum at $\nu \approx 473\ cm^{-1}$ that, according to Yashima's reference data,[12] is attributed to a $t''$-like phase with $x$ close to 0.7. The most characteristic band of the low $x$, tetragonal phase is still observed at ~245 $cm^{-1}$, thus implying that segregation yields $t + t''$ phases, instead of the $t + c$ decomposition expected from equilibrium PD.

On increasing $T_a$ this trend is further enhanced. For $T_a$ = 1450 °C, the spectral shape in the region 450–600 $cm^{-1}$ is typical of $t'$ phase with $x$ = 0.6, whereas the band of the $t$-phase is found at an almost fixed position, thus implying segregation into $t(0.18–0.2) + t'(0.6)$ phases. For $T_a$ = 1500 °C the band arising from the stable $t$ phase has lost half of its intensity and the $t'$-like spectrum corresponds to $x \approx 0.5–0.55$ content. Finally, for $T_a$ = 1650 °C, the stable $t$-phase is only weakly present, and a mostly $t'$-like spectrum is found, pertaining to a Ce content ($x \approx 0.42$) close to the nominal one.

Instead of looking at a fixed composition and varying $T_a$, we may apply a "transverse" look and see how phases vary as a function of nominal composition for fixed $T_a$. Thus, for $T_a$ = 1500 °C we find the spectra shown in Fig. 5. No cubic, Ce-rich phase is

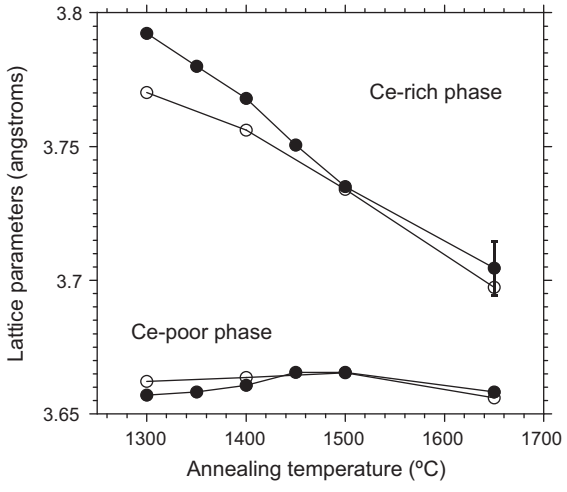


Fig. 3. Lattice parameters of the Ce-rich and Ce-poor phases segregated in samples produced by solid state reaction (black symbols) and by a modified Pechini method (open symbols) (Ref. 10). For tetragonal phases, the pseudocubic average is plotted. The error bar for the ceramic sample annealed at 1650 °C is due to the presence of a third, cubic phase with large lattice parameter.

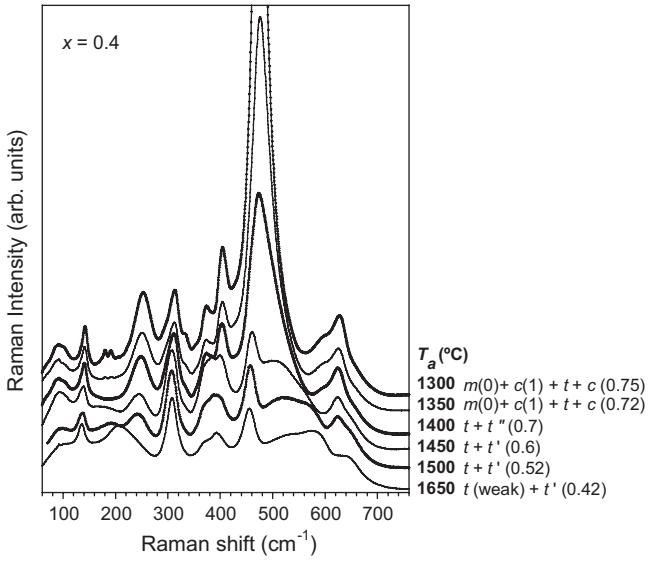


Fig. 4. Evolution of the Raman spectrum of nominally $Zr_{0.6}Ce_{0.4}O_2$ oxide as a function of annealing temperature $T_a$. The phase content determined from Raman spectra is indicated on the right. The composition of the stable tetragonal varies weakly within $x_t \approx 0.18–0.2$ (see text).

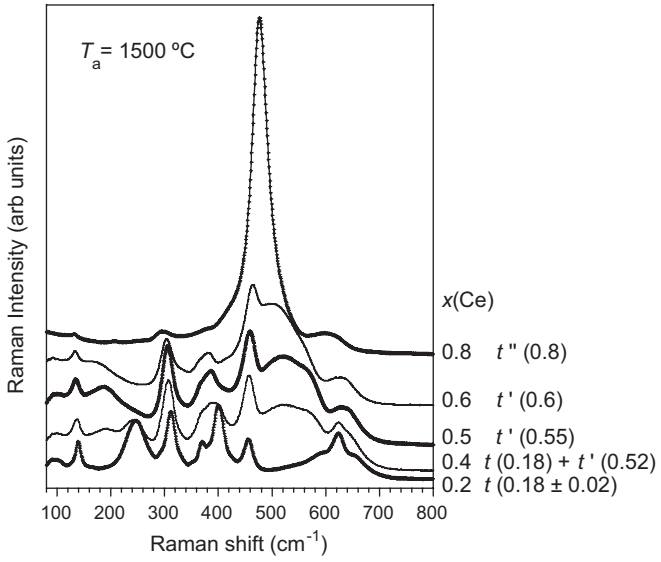


Fig. 5. Raman spectra of $Zr_{1-x}Ce_xO_2$ samples annealed at 1500 °C. The Ce composition $x$ is indicated on the right of the figure, together with the phase content determined from the spectra.

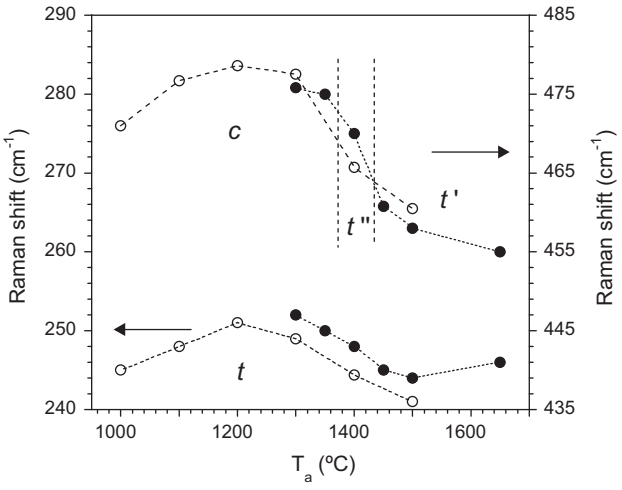


Fig. 7. The Raman shifts of the pseudocubic band of the Ce-rich phase (upper data) and of the band characteristic of the Ce-poor tetragonal phase (lower data) are plotted with filled symbols as a function of annealing temperature. Data from sol–gel produced samples (see Ref. 10) are included for comparison (open symbols). Error bars in Raman shifts are ±1 $cm^{-1}$.

formed at this temperature, in apparent contradiction with the PD. Instead, and depending on composition, we find a $t''$-like spectrum as a single phase for $Ce_{0.8}$, a $t'$-like spectrum pertaining to $x = 0.6$, also as a single phase, for composition $Ce_{0.6}$, and a weak segregation effect for $Ce_{0.5}$ in the form of a minority $t$(0.18–0.2) phase plus a majority $t'$(0.55) phase. Phase segregation also occurs for $Ce_{0.4}$ into a (now more intense) $t$ phase and a $t'$ phase with $x \approx 0.52$. Finally, almost pure $t$ phase is found for $Ce_{0.2}$, within the sensitivity limits of Raman experiments.

The same type of experiment but with $T_a = 1650$ °C yields spectra shown in Fig. 6. At this temperature, the $Ce_{0.4}$ composition segregates into $t$(weak) + $t'$(≈0.42). For higher Ce content, single phases are found with composition very close to the

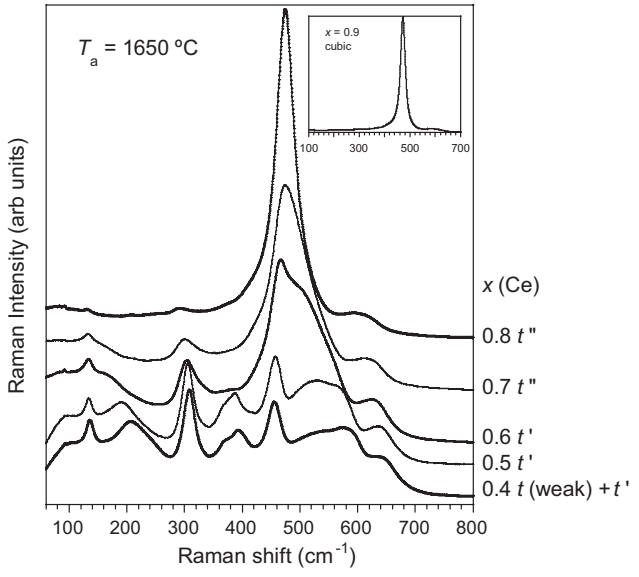


Fig. 6. Raman spectra of $Zr_{1-x}Ce_xO_2$ samples of varying composition annealed at 1650 °C.

nominal one: $t'$ for 0.5 and 0.6, and $t''$ for 0.7 and 0.8. For $Ce_{0.9}$ the intense band of cubic fluorite is found, with no intensity at 300 $cm^{-1}$, suggesting that a true cubic phase is formed for this composition.

The identification of the Ce-rich segregated phase is mainly based on the comparison of the shape and frequency of the cubic or pseudocubic band with reference data.[12] This band appears at $\nu_c = 465$ $cm^{-1}$ in pure $CeO_2$ and its frequency increases with decreasing $x$ as far as the structure remains cubic, due to lattice compression. Below $x \sim 0.85$, however, the structure becomes tetragonal and the band splits into three components. We shall use the notation $\nu_c$ for the frequency of the most intense component, which is the one appearing at lowest frequency. For that band, the relation between $\nu_c$ and Ce content is reversed, i.e., lower $\nu_c$ corresponds to *lower* Ce-content.[12]

The composition of the Ce-poor tetragonal phase can be determined from the frequency of the characteristic band around 250 $cm^{-1}$ ($\nu_t \sim 263$ $cm^{-1}$ for pure $t$-$ZrO_2$ at high temperature[27]) and the shape of the PD in the low Ce-content region.

$\nu_c$'s and $\nu_t$'s are plotted in Fig. 7 as a function of the annealing temperature. Data from samples synthesized by a modified Pechini method[10] are also included for comparison. Pechini samples, with nominal composition $Zr_{0.5}Ce_{0.5}O_2$, were annealed for 2 h at temperatures from 1000 to 1500 °C, i.e., in the $t + c$ phase field. As Fig. 6 of Ref. 10 shows, between 1000 and 1300 °C the Ce-rich segregated phase of Pechini samples has a cubic fluorite spectrum, whereas for $T_a = 1400$ and 1500 °C the metastable $t''$ and $t'$ phases form, respectively, in agreement with the trend of materials sintered by standard ceramic methods. Though the phases formed in these samples are qualitatively the same as in ceramic powders, Raman frequencies shown in Fig. 7 reveal small but significant shifts between both series. This behavior can be discussed in relation with the difference in lattice parameters determined from XRD (Fig. 3 and Ref. 10).

For all annealing temperatures used, ceramic samples show *higher* $\nu_t$'s than Pechini samples, which, according to the relation between $\nu_t$ and Ce content, would imply slightly *lower* Ce content in the ceramic samples. This behavior is in agreement with the smaller cell volume found for the Ce-poor phase in the ceramic samples and may be ascribed to incomplete phase segregation in Pechini samples, due to the short annealing times (2 h) used in Ref. 10. As reaction progresses with longer retention time, the Ce content of the Ce-poor phase is reduced, resulting in higher $\nu_t$ in ceramic samples, as observed.

The behavior of the characteristic frequency of the Ce-rich phase, $\nu_c$, is more subtle and is, apparently, not systematic. At 1300 °C, $\nu_c$ (ceramic) < $\nu_c$ (Pechini); at 1400 °C the opposite is true and, at 1500 °C, lower $\nu_c$ is again found for ceramic samples. The explanation has to be made point by point in relation with the PD and the behavior expected at increasing annealing temperatures. If incomplete segregation occurs in Pechini samples, one would expect lower Ce-content for the Ce-rich phase in the Pechini series, and in fact at 1300 °C the lattice parameter of the Pechini sample is smaller than that of the ceramic sample (see Fig. 3). Since at this temperature the Ce-rich phase is still cubic, a smaller lattice parameter implies a higher frequency for the quasicubic mode, which explains why $\nu_c$ (Pechini) > $\nu_c$ (ceramic). On annealing at 1400 °C and above, however, the Ce-rich phase adopts the tetragonal $t''$ phase, first, and then the $t'$ phase, for which the relation between $\nu_c$ and Ce content is reversed. Then, the higher $\nu_c$ of the ceramic sample annealed at 1400 °C agrees with the larger pseudocubic lattice parameter shown in Fig. 3 and thus a higher Ce content which is again attributed to incomplete equilibrium of Pechini samples. On further increasing $T_a$ the lattice parameters of Pechini and ceramic samples tend to converge, despite the difference in annealing times, in agreement with the expectation that increasing temperature favors diffusion processes and thus enhances segregation. (The large error bar of the ceramic sample annealed at 1650 °C is due to the presence of a third, cubic phase, which may arise from partial segregation of the Ce-rich phase upon cooling, thus modifying the composition and lattice parameter of the main t′ phase.)

Determining the Ce content of the Ce-poor phase is difficult, since data for compositions below $x \sim 0.2$ are lacking in Ref. 12. Moreover, the value given in that work for $Ce_{0.2}$ ($\nu_t = 230\ cm^{-1}$) is much lower than those usually reported. According to the PD, in the 1300–1650 °C temperature interval the composition of the Ce-poor phase hardly varies between 0.18 and 0.2. On the other hand, we find a significant variation of $\nu_t$ of about 10 $cm^{-1}$ in the same interval, which would imply either that the $\nu_t(x)$ relation is very steep around $x = 0.2$, or that the variation of Ce content is greater than only 2%. We shall discuss this point in next section.

## 4. Discussion

According to the equilibrium phase diagram of the $ZrO_2$–$CeO_2$ system,[11] above 1050 °C and for $CeO_2$ content between 15% and 85%, phase segregation is expected to give a Ce-poor phase, with the stable tetragonal structure and Ce composition varying only slightly between 15% and 20%, and a Ce-rich phase, with the cubic fluorite structure and Ce content decreasing quickly as temperature increases.

The experimental results presented here indicate that for $T_a = 1300$ and 1350 °C the segregated phases are those predicted by the equilibrium PD: the Ce-poor phase is a tetragonal phase with $x \approx 0.18$, and the Ce-rich phase is a cubic fluorite whose Raman shift increases with increasing Zr amount, due to lattice contraction. However, for sintering temperatures at, or above, 1400 °C, the Ce-rich phase is not the expected cubic fluorite: at 1400 °C a metastable $t''$-phase is found, whereas for $T_a = 1450$, 1500 and 1650 °C the also metastable $t'$ phase forms. The compositions of the Ce-rich segregated phases are plotted, together with the PD, in Fig. 1.

We ascribe the presence of metastable $t'$ or $t''$ phases in the Ce-rich side of the segregated phases to partial Ce reduction: it is well-known that $Ce^{4+}$ tends to be reduced to $Ce^{3+}$ at high temperatures, typically above 1400 °C in air atmosphere. To maintain charge neutrality, a corresponding percentage of oxygen vacancies must be formed. $Ce^{3+}$, with its higher ionic radius, acts exactly as $Y^{3+}$ in YSZ and produces a cubic, defective phase, which can be quenched upon fast cooling. (In this context, defective or non-defective refers to the presence or absence of oxygen vacancies.)

In Yashima's works this phase is labeled as $c'$ and is ascribed to either the cubic fluorite or the pseudocubic $t''$-phase, that has $c = a$ but with oxygen displacement $O(z) \neq 0$. In fact, we should distinguish between defective and non-defective $c'$ phases, depending on whether the oxygen partial pressure may produce Ce reduction or not. Non-defective $c'$-phase can be, depending on sample composition and thermal history, either stable cubic fluorite or pseudocubic metastable $t''$-phase. On the other hand, defective $c'$, which forms under partially reducing conditions, has random oxygen vacancies but no long-range ordered oxygen displacements, according to high temperature neutron scattering experiments on $Zr_{0.5}Ce_{0.5}O_2$.[28] Therefore, the defective $c'$-phase must be ascribed to a defect fluorite (DF) phase.

In consequence, for $T_a < 1400$ °C the high temperature phase labeled as "cubic" will be a non-defective, though cation-disordered cubic fluorite, whereas for $T_a > 1400$ °C the cubic phase will be a defect fluorite with random distribution of $Zr^{4+}$, $Ce^{4+}$, $Ce^{3+}$ and oxygen vacancies.

Though the $ZrO_2$–$CeO_2$ PD assumes that all Ce ions are in $Ce^{4+}$ state, the ternary $ZrO_2$–$CeO_2$–$Ce_2O_3$ PD should be strictly considered. If reduction effects are weak, the binary diagram may be used, but having in mind that above a certain temperature the high temperature cubic phase will be a defective phase.

At this point, it is worth to recall that XRD gives only the average structure, which may differ from the local structure if there exist short-range ordered regions with a correlation length smaller than that given by XRD. On the other hand, Raman scattering is sensitive to both long and short-range structures, so that Raman spectra frequently denote lower symmetry than XRD in disordered systems. Thus, the defective $c'$-phase is assumed to be a defect fluorite *at the XRD level*, in the same sense as YSZ is assumed to be a cubic fluorite though its Raman spectrum is not characteristic of a cubic fluorite. In fact, a very

defective $Zr_{0.6}Ce_{0.4}O_{2-\delta}$ sample produced from the melt by the laser floating zone technique, with a cubic diffractogram, showed a broad Raman spectrum which, however, resembled more a tetragonal spectrum than a cubic one.[29] It is thus very likely that $t'$ or $t''$-like oxygen displacements are already present, at a short-range scale, in the defective $c'$-phase, and that these displacements become long-range ordered on subsequent reoxidation.

Based on these considerations, we propose the following picture to explain our results: during the annealing procedure above 1400 °C, phase segregation occurs in the form of $t$ + defective-$c'$ (DF). Cooling rates used in this work are fast enough to maintain the phase compositions established at the annealing temperature but are slow enough to allow oxygen diffusion and reoxidation. Then, the defective phase segregated at $T_a$ will transform upon cooling to either $t'$ or $t''$ phase, depending on its Ce content, so that we observe, at RT, $t + t'$ or $t + t''$ segregation.

The composition of the Ce-rich phase formed in the 1400–1650 °C range is lower than would correspond to the non-defective cubic phase at each temperature, according to the equilibrium PD. This is reflected in Fig. 1, where we plot the compositions found in this work compared to the predictions of the PD. The shift of the Ce-rich phase composition is ascribed to partial Ce reduction, which widens the high-temperature cubic phase field toward lower Ce content and thus lowers the $c \rightarrow t + c$ or $c' \rightarrow t'$ transition temperatures, as already noted by Yashima et al.[14] Quite interestingly, for $T_a = 1650$ °C the shift of the Ce-rich phase composition is very small, indicating, in agreement with previous reports, that Ce can be reduced more easily at the intermediate than at the end compositions of $Zr_{1-x}Ce_xO_2$.[4] The explanation of that behavior is that Ce reduction requires oxygen diffusion, which is maximized in the highly disordered intermediate compositions.

Though it seems that the stable tetragonal phase, with only ~20% cerium content, can afford a certain $Ce^{3+}$ content quite easily, a priori some effect might be expected due to partial reduction at high temperatures. In fact, $\nu_t$ shifts from 253 $cm^{-1}$ for $T_a = 1300$ °C to only 243 $cm^{-1}$ for $T_a = 1500$ °C (see Fig. 7), which might be attributed to lattice expansion induced by $Ce^{3+}$, if we assume that the composition of the stable $t$-phase remains almost fixed in this temperature range. In that case, however, the upturn of $\nu_t$ for $T_a = 1650$ °C would be difficult to explain. Alternatively, frequency shifts might also be attributed to small composition variation, as predicted by the PD, and subsequent change of lattice parameter. The downshift of $\nu_t$ between 1300 and 1500 °C could be due to $x_t$ increasing, whereas the upturn of $\nu_t$ at 1650 °C can be ascribed to the shift of $x_t$ toward lower concentrations at higher temperatures (see the PD in Fig. 1).

We now discuss our results in relation with Yashima's experiments and the stable/metastable PD. A first difference is the thermal treatment applied to the samples: whereas Yashima quenches the annealed samples from the cubic field of the PD, i.e., from regions with no phase segregation, and submits them afterwards to mild reoxidation, our samples are equilibrated for long annealing times at temperatures that correspond, for certain compositions, to within the $t + c$ field, allowing for full phase separation in the form of $t$ + DF or $t + c$, depending on whether $T_a$ is higher or lower than 1400 °C. In Yashima's PD the transitions from $t'$ to $t''$ and then from $t''$ to cubic phase are indicated by dashed lines. These temperatures were obtained by heating the non-defective $t'$ samples for short periods of only 3 min, in order to avoid phase separation and Ce reduction. In those conditions, non-defective $c'$ phase (after identified as $t''$-phase) is first formed, that subsequently will transform to either defective or non-defective cubic fluorite phase. In the present work, on the contrary, long annealing times are employed, so that full phase separation is let to occur.

## 5. Summary and conclusions

We have applied Raman spectroscopy to study phase segregation of $Zr_{1-x}Ce_xO_2$ samples submitted to long annealing times at temperatures between 1300 and 1650 °C.

For $Zr_{0.6}Ce_{0.4}O_2$, Raman spectra measured at RT show superposition of spectra corresponding to two phases: a tetragonal phase with Ce content around 0.18 and a Ce-rich phase whose composition varies rapidly as a function of annealing temperature. If 1300 °C < $T_a$ < 1400 °C, spectra can be interpreted as arising from $t + c$ segregation, in agreement with the equilibrium PD. However, for $T_a \geq 1400$ °C, the spectrum of the Ce-rich phase is not that of a cubic fluorite. The following sequence of segregated phases is found: $t + t''(0.7)$ at 1400 °C; $t + t'(0.6)$ at 1450 °C, $t + t'(0.52)$ at 1500 °C and almost single $t'(\sim 0.42)$ phase at 1650 °C. The compositions of the Ce-rich metastable phases thus formed are lower than would correspond to the non-defective cubic fluorite phase.

The presence of metastable phases in the Ce-rich side of the segregated phases and the shift of their compositions, as compared with the predictions of the equilibrium PD, are ascribed to partial Ce reduction above 1400 °C. $Ce^{3+}$ ions expand the lattice and allow oxygen displacements that drive the formation of metastable $t'$ and $t''$ phases upon reoxidation at low temperatures. In fact, lattice expansion is the common factor that leads to metastable phases either in low temperature synthesis or in samples annealed at high temperature under partially reducing atmosphere. In nano-sized systems expansion is due to surface effects and associated lattice strain, whereas in partially reduced compounds expansion comes from the higher ionic radius of $Ce^{3+}$ compared to $Ce^{4+}$.

The following picture emerges: long annealing times within the $t + c$ field allow for full phase separation in the form of $t$ + DF or $t + c$, depending on whether $T_a$ is higher or lower than 1400 °C. The defect fluorite phases segregated when $T_a \geq 1400$ °C transform upon cooling to either $t'$ or $t''$ phase, depending on their Ce content. This explains the finding, at RT, of apparent segregation of the form $t + t'$, $t + t''$ or $t + c$.

No pyrochlore-like phases are detected in this work, suggesting that reduction conditions are not severe enough to yield, even at the highest temperatures used, $Zr^{4+}/Ce^{3+}$ cation ordered configurations.

Our findings may have some implications in relation with the technological use of ZCO materials. In particular, they may help for an understanding of the mechanisms behind the phase conversion upon consecutive reduction and

reoxidation treatments.[18,19] For increasingly reducing atmosphere, the composition of the Ce-rich metastable phase will shift toward lower Ce content, eventually leading, depending on the nominal composition and annealing temperature, to a single defective phase for compositions that would segregate in non-reducing atmospheres. In fact, this explains the formation of pyrochlore $Ce_2Zr_2O_{7+\delta}$ after severe reduction of $t'$-$Ce_{0.5}Zr_{0.5}O_2$ at 1300 °C for as long as 10 h without segregation.[18]

## Acknowledgements

This work was supported by Spanish CICYT through MAT2010-19837-C06-06 grant and Feder funds.

## References

1. Yuan Q, Duan HH, Li LL, Sun LD, Zhang YW, Yan CH. Controlled synthesis and assembly of ceria-based nanomaterials. *Journal of Colloid and Interface Science* 2009;**335**:151–67.
2. Kaspar J, Fornasiero P, Graziani M. Use of $CeO_2$-based oxides in the three-way catalysis. *Catalysis Today* 1999;**50**:285–98.
3. Trovarelli A, editor. *Catalysis by ceria and related materials*. *Catalytic science series*, vol. 2. London: Imperial College Press; 2002.
4. Fornasiero P, Di Monte R, Ranga Rao G, Kaspar J, Meriani S, Trovarelli A, et al. Rh-loaded $CeO_2$–$ZrO_2$ solid–solutions as highly efficient oxygen exchangers: dependence of the reduction behavior and the oxygen storage capacity on the structural-properties. *Journal of Catalysis* 1995;**151**:168–77.
5. Hori CE, Permana H, Simon KY, Brenner NgA, More K, Rahmoeller KM, et al. Thermal stability of oxygen storage properties in a mixed $CeO_2$–$ZrO_2$ system. *Applied Catalysis B* 1998;**16**:105–17.
6. Kaspar J, Fornasiero P. Nanostructured materials for advanced automotive de-pollution catalysts. *Journal of Solid State Chemistry* 2003;**171**:19–29.
7. Mamontov E, Brezny R, Koranne M, Egami T. Nanoscale heterogeneities and oxygen storage capacity of $Ce_{0.5}Zr_{0.5}O_2$. *Journal of Physical Chemistry B* 2003;**107**:13007–14.
8. Colón G, Valdivieso F, Pijolat M, Baker RT, Calvino JJ, Bernal S. Textural and phase stability of $Ce_xZr_{1-x}O_2$ mixed oxides under high temperature oxidising conditions. *Catalysis Today* 1999;**50**:271–84.
9. Di Monte R, Kaspar J. Nanostructured $CeO_2$–$ZrO_2$ oxides. *Journal of Materials Chemistry* 2005;**15**:633–48.
10. Várez A, Jolly J, Oliete P, Sanjuán ML, García-González E, Jardiel T, et al. Multiphase transformations controlled by Ostwald's rule in nanostructured $Ce_{0.5}Zr_{0.5}O_2$ powders prepared by a modified Pechini route. *Inorganic Chemistry* 2009;**48**:9693–9.
11. Yashima M, Morimoto K, Ishizawa N, Yoshimura M. Diffusionless tetragonal-cubic transformation temperature in zirconia–ceria solid solutions. *Journal of the American Ceramic Society* 1993;**76**:2865–8.
12. Yashima M, Arashi H, Kakihana M, Yoshimura M. Raman scattering study of cubic-tetragonal phase transition in $Zr_{1-x}Ce_xO_2$ solid solution. *Journal of the American Ceramic Society* 1994;**77**:1067–71.
13. Yashima M, Takashina M, Kakihana M, Yoshimura M. Low-temperature phase equilibria by the flux method and the metastable-stable phase diagram in the $ZrO_2$–$CeO_2$ system. *Journal of the American Ceramic Society* 1994;**77**:1869–74.
14. Yashima M, Morimoto K, Ishizawa N, Yoshimura M. Zirconia–Ceria solid solution synthesis and the temperature–time-transformation diagram for the 1:1 composition. *Journal of the American Ceramic Society* 1993;**76**:1745–50.
15. Yashima M, Kakihana M, Yoshimura M. Metastable-stable phase diagrams in the zirconia-containing systems utilized in solid-oxide fuel cell application. *Solid State Ionics* 1996;**86–88**:1131–49.
16. Yashima M, Hirose T, Katano S, Suzuki Y, Kakihana M, Yoshimura M. Structural changes of $ZrO_2$–$CeO_2$ solid solutions around the monoclinic-tetragonal phase boundary. *Physical Review B* 1995;**51**:8018–25.
17. Zhang F, Chen C-H, Hanson JC, Robinson RD, Herman IP, Chan S-W. Phases in ceria–zirconia binary oxide $(1-x)CeO_2$–$xZrO_2$ nanoparticles: the effect of particle size. *Journal of the American Ceramic Society* 2006;**89**:1028–36.
18. Omata T, Kishimoto H, Otsuka-Yao-Matsuo S, Ohtori N, Umesaki N. Vibrational spectroscopic and X-ray diffraction studies of cerium zirconium oxides with Ce/Zr composition ratio = 1 prepared by reduction and successive oxidation of $t'$-$(Ce_{0.5}Zr_{0.5})O_2$ phase. *Journal of Solid State Chemistry* 1999;**147**:573–83.
19. Montini T, Hickey N, Fornasiero P, Graziani M, Bañares MA, Martínez-Huerta MV, et al. Variations in the extent of pyrochlore-type cation ordering in $Ce_2Zr_2O_8$: a $t'$-$\kappa$ pathway to low-temperature reduction. *Chemistry of Materials* 2005;**17**:1157–66.
20. Fornasiero P, Balducci G, Di Monte R, Kaspar J, Sergo V, Gubitosa G, et al. Modification of the redox behaviour of $CeO_2$ induced by structural doping with $ZrO_2$. *Journal of Catalysis* 1996;**164**:173–83.
21. Yashima M, Ohtake K, Arashi H, Kakihana M, Yoshimura M. Determination of cubic-tetragonal phase boundary in $Zr_{1-x}Y_xO_{2-x/2}$ solid solutions by Raman spectroscopy. *Journal of Applied Physics* 1993;**74**:7603–5.
22. Várez A, García-González E, Jolly J, Sanz J. Structural characterization of $Ce_{1-x}Zr_xO_2$ $(0 \le x \le 1)$ samples prepared at 1650 °C by solid state reaction. A combined TEM and XRD study. *Journal of the European Ceramic Society* 2007;**27**:3677–82.
23. Montini T, Speghini A, De Rogatis L, Lorenzut B, Bettinelli M, Graziani M, et al. Identification of the structural phases of $Ce_xZr_{1-x}O_2$ by Eu(III) luminescence studies. *Journal of the American Chemical Society* 2009;**131**:13155–60.
24. Hirata T, Asari E, Kitajima M. Infrared and Raman spectroscopic studies of $ZrO_2$ polymorphs doped with $Y_2O_3$ or $CeO_2$. *Journal of Solid State Chemistry* 1994;**110**:201–7.
25. Rodriguez-Carvajal J. Recent advances in magnetic structure determination by neutron powder diffraction. *Physica B* 1993;**192**:55.
26. Fornasiero P, Speghini A, Di Monte R, Bettinelli M, Kaspar J, Bigotto A, et al. Laser-excited luminescence of trivalent lanthanide impurities and local structure in $CeO_2$–$ZrO_2$ mixed oxides. *Chemistry of Materials* 2004;**16**:1938–44.
27. Phillipi CM, Mazdiyas KS. Infrared and Raman spectra of zirconia polymorphs. *Journal of the American Ceramic Society* 1971;**54**:254.
28. Wakita T, Yashima M. In situ observation of the tetragonal-cubic phase transition in the $CeZrO_4$ solid solution – a high temperature neutron diffraction study. *Acta Crystallographica Section B: Structural Science* 2007;**63**:384–9.
29. Sanjuán ML, Oliete PB, Várez A, Sanz J. Structural and spectroscopic characterization of $Ce_{0.4}Zr_{0.6}O_2$ crystalline rods grown by the laser floating zone method. *Boletín de la Sociedad Española de Cerámica y Vidrio* 2008;**47**:165–70.